The Effects of Extraframework Species on the Structure-Based Prediction of ^{31}P Isotropic Chemical Shifts of Aluminophosphates

Daniel M. Dawson*, Valerie R. Seymour and Sharon E. Ashbrook*

School of Chemistry, EaStCHEM and St Andrews Centre for Magnetic Resonance, University of St Andrews, North Haugh, St Andrews KY16 9ST, UK

ABSTRACT: ^{31}P NMR spectroscopy is a valuable technique for the characterization of the local structure of aluminophosphates (AlPOs), capable of providing information on the number of crystallographic P sites, their relative populations, and the positions of any dopant atoms in the framework. Assigning the ^{31}P spectra may, however, require multinuclear NMR experiments and/or density functional theory (DFT) calculations, which can be time consuming, computationally costly, and challenging in cases involving disorder or dynamics. To address the issue of computational cost, we recently demonstrated a simple relationship between the local structure around P (primarily in terms of the mean P-O bond length and P-O-Al bond angle) and the ^{31}P isotropic chemical shift, δ_{iso}, calculated by DFT for a series of calcined AlPOs. Here, we extend this approach to as-made AlPOs where we show that, at least to a first approximation, the presence of framework-bound anions and/or guest species within the pores of AlPOs can be translated directly to a distortion of the local framework geometry without considering any additional structural parameters. This allows the prediction of a DFT-level ^{31}P δ_{iso} even in cases where the structure may be highly disordered or partially incomplete (precluding the use of electronic structure calculations), and we investigate the minimal structural information required to provide meaningful results. The structure-spectrum relationship produced forms the basis for the geometry-based DIStortion COde (DISCO), which can rapidly (on the ms timescale) predict the outcome of a DFT calculation of ^{31}P δ_{iso} to within 1.1 ppm.

Introduction

Microporous aluminophosphates (AlPOs) are well-known materials comprising three-dimensional networks of alternating corner-sharing AlO_4 and PO_4 tetrahedra, giving a neutral $AlPO_4$ framework.[1,2] The synthesis of a specific framework type can be guided by the use of a cationic organic structure directing agent (SDA), and an anionic mineralizer (typically HO^- or F^-), both of which are incorporated within the "as-made" material, with the charge of the SDA cations within the pores balanced by the anions, which bind to the framework to give five- or six-coordinate Al (Al^V and Al^{VI}, respectively) in addition to the expected tetrahedral Al^{IV}.[1,2]

Since their discovery, solid-state NMR spectroscopy has been recognized as a useful tool for the structural characterization of AlPOs, owing to the large number of NMR-active nuclei present, with ^{27}Al and ^{31}P particularly commonly studied owing to their high sensitivity.[3,4] ^{31}P (spin I = 1/2, 100% natural abundance) NMR spectra can provide much information, including the number of distinct P species present, their relative populations and, in doped materials, information on the amount and distribution of the dopant atoms may be determined (much of this information is also present in the ^{27}Al NMR spectra, but typically obscured by the second-order quadrupolar interaction arising from the higher spin quantum number (I = 5/2) of this nucleus).[4-8] In the early days, ^{31}P NMR spectra of AlPOs were typically assigned using the relationship between mean P-O-Al bond angle $\langle\theta_{POAl}\rangle$ and ^{31}P isotropic chemical shift (δ_{iso}) proposed by Müller *et al*.[9] based on the NMR parameters of three dense $AlPO_4$ phases (later refined by Kanehashi *et al*., using three calcined AlPOs to give a dataset of 10 unique P species[10]). More recently, periodic density functional theory (DFT) calculations have superseded this simple empirical approach, owing to their ability to calculate accurate NMR parameters for a given crystal structure or structural model (although good agreement with experiment is often achieved only after the structure has been optimized to minimize atomic forces).[11-14] However, DFT calculations on AlPOs, particularly containing dopant atoms within the framework or mobile guest species within the pores (*i.e.,* in industrially-relevant cases such as catalysis or gas separation), can be computationally expensive and typically require many hours of high-performance computing time. In addition, the results of DFT calculations, while providing an accurate assignment of the NMR spectrum, do not always provide a clear rationale for *why* the NMR spectrum appears as it does. This point is particularly problematic in the case of microporous materials such as AlPOs, where the idea of "rational design" of frameworks for specific applications is very popular and the ability to relate changes in NMR spectra directly to changes in specific structural features has the potential to be of great use for indicating which types of structural feature need to be included or avoided. In recent work, we exploited the recent advances in computation and revisited the relationship between $\langle\theta_{POAl}\rangle$ and the DFT-calculated ^{31}P isotropic shielding, σ_{iso}^{DFT}, (linearly related to δ_{iso}, as discussed below) for calcined AlPOs and showed that, when the mean P-O bond length, $\langle r_{PO}\rangle$, was

considered in addition to $\langle\theta_{POAl}\rangle$, the value of σ_{iso}^{DFT} calculated by the periodic CASTEP code[15] could be predicted simply from the local structure with a mean absolute error (MAE) of 1.6 ppm.[16] The improved accuracy of this approach over earlier structure-based spectral predictions likely arises from the elimination of the experimental uncertainty inherent in previous work (*i.e.*, by comparing DFT-calculated shifts to exactly known structures) and the consideration of more than one structural parameter as influencing δ_{iso}. While our earlier work represents a more accurate approach than that of Müller *et al*., and a more rapid approach than DFT, the study was confined to calcined AlPOs, in which the SDA, anions, and any water within the pores are removed by heating, leaving only the tetrahedral $AlPO_4$ framework.

In this work, we investigate the factors that must be considered in order to extend our earlier methodology to the prediction of NMR parameters for the more complex as-made AlPOs. We demonstrate that good agreement between the ^{31}P σ_{iso} calculated by DFT and that predicted from the geometry of a structural model can be achieved by assuming that (to a first approximation) all structural distortions induced by the SDA, framework-bound anions and $Al^{V/VI}$ within the framework manifest simply as changes to $\langle\theta_{POAl}\rangle$ and $\langle r_{PO}\rangle$. This work paves the way for a new code that can rapidly predict the ^{31}P δ_{iso} for any given structural model. This program, called the DIStortion COde (DISCO), could find application in high-throughput calculations for, *e.g.*, screening potential structural models and/or molecular dynamics (MD) runs that would be inaccessible to DFT on current computing hardware.

Computational and Experimental Details

All crystal structures were taken from the literature (see below and the Supporting Information (S1) for further details and references). For some, the unit cell parameters and atomic coordinates were optimized to minimize the forces acting on the atoms prior to calculation of the NMR parameters. All DFT calculations used the CASTEP code (version 5.5.2),[15] employing the GIPAW algorithm[17] to reconstruct the all-electron wavefunction in the presence of a magnetic field. Calculations were performed using the GGA PBE functional, with core-valence interactions described by ultrasoft pseudopotentials.[18] A planewave energy cut off of 60 Ry (816 eV) was used, and integrals over the Brillouin zone were performed using a Monkhurst-Pack grid with a k-point spacing of 0.04 2π Å^{-1}. Dispersion interactions were reintroduced using the scheme of Tkatchenko and Scheffler,[19] as implemented by McNellis *et al*.[20] Calculations were performed on a 198-node (2376 core) Intel Westmere cluster with 2 GB memory per core and QDR Infiniband interconnects at the University of St Andrews. Calculations generate the absolute shielding tensor, $\boldsymbol{\sigma}$, in the crystal frame. From the principal components of the symmetric part of $\boldsymbol{\sigma}$ it is possible to generate the isotropic shielding, σ_{iso} = (1/3) Tr{$\boldsymbol{\sigma}$}. The isotropic chemical shift is given (assuming $\sigma_{ref} \ll 1$) by $\delta_{iso}^{DFT} = -\left(\sigma_{iso} - \sigma_{ref}\right)/m$, where σ_{ref} is a reference shielding, here 274.38 ppm for ^{31}P. The scaling factor, m, is ideally 1 but, here a value of 1.1576 was used. The values for σ_{ref} and m were determined by comparing experimental and calculated chemical shifts for AlPO-14(ipa), AlPO-14(calc) and SIZ-4.[11,21]

Structure-spectrum relationships and the uncertainties in the coefficients determined were obtained using the MATLAB[23] routines described previously.[16,24] All values calculated by MATLAB are given to higher precision in the Supporting Information (S2).

Structural parameters were obtained using the (in house) FORTRAN 90 DIStortion COde (DISCO).[22] DISCO then uses these structural parameters to predict the ^{31}P chemical shift, δ_{iso}^{DISCO} based on the prediction of σ_{iso} from Eq. 3 below and the referencing described above. The source code and user guide for the current version (DISCO 17.1) are included in the Supporting Information (S4). Calculations were performed using the EaStCHEM Research Computing Facility, comprising a 54-node (1728-core) Intel Broadwell cluster with 4 GB memory per core and FDR Infiniband interconnects at the University of St Andrews.

The ^{31}P NMR spectra were recorded on a Bruker Avance III spectrometer equipped with a 14.1 T wide-bore superconducting magnet. The samples were packed into 4 mm (STA-2) or 3.2 mm (calcined hydrated AlPO-34) zirconia rotors and rotated at the magic angle at a rate of 10-14 kHz. Signal averaging was carried out for 80 transients with a recycle interval of 10 s (STA-2) or 4 transients with a recycle interval of 120 s (calcined hydrated AlPO-34). Chemical shifts are reported in ppm relative to 85% aqueous H_3PO_4, using BPO_4 (δ = –29.6 ppm) as a secondary solid reference.

Results and Discussion

Calcined AlPOs

Table 1 summarizes the ordered as-made and calcined AlPOs considered in this work, with further details given in the Supporting Information (S1). As it is often necessary to optimize the experimental structures of AlPOs in order to obtain calculated NMR parameters in good agreement with experiment,[11,13,42] this was carried out for all structures listed in Table 1. Sneddon *et al*. showed that, for AlPOs, the precise optimization method is not particularly important in terms of the accuracy of the NMR parameters and the local structures obtained, but that the inclusion of longer-range dispersive interactions yielded structures in better general agreement with the crystallographic measurements.[13] Therefore, in this work, the semi-empirical dispersion-correction scheme of Tkatchenko and Scheffler[19] was used to reintroduce the dispersive interactions in all structural optimizations.

In previous work, it was shown, for a series of calcined AlPOs taken from the literature, that the ^{31}P isotropic shielding calculated by DFT (σ_{iso}^{DFT}) could be predicted from the mean P-O bond lengths, $\langle r_{PO}\rangle$, and mean P-O-Al bond angles, $\langle\theta_{POAl}\rangle$, using

$$\sigma_{iso} = 0.8980\left\langle\theta_{POAl}\right\rangle - 1190\left\langle r_{PO}\right\rangle^2 + 3320\left\langle r_{PO}\right\rangle - 2120 \quad , \quad (1)$$

where bond angles are in degrees, bond lengths in Å and all coefficients have units such that σ_{iso} is in ppm.[16] This relationship provided values of σ_{iso} that agreed with σ_{iso}^{DFT} to within a MAE of 0.5 ppm for three test structures, although it is possible that the MAE for a larger data set would be greater, as a value of 1.6 ppm was observed for the training set (which contained a wider range of bond lengths and angles than the test set). As observed previously, neither $\langle r_{PO}\rangle$ nor $\langle\theta_{POAl}\rangle$ alone

Table 1. Summary of the ordered AlPO structures used. All structures were optimized prior to calculation of the NMR parameters. Further details are given in the text and Supporting Information (S1).

AlPO	Framework type[25]	SDA	Anion	Ref.
as-made AlPOs				
SIZ-4	CHA	1,3-dimethylimidazolium	F^-	26, 27
AlPO-34(morph)	CHA	morpholinium	F^-	28
AlPO-15	–	ammonium	OH^-	29
AlPO-14(ipa)	AFN	*iso*propylammonium	OH^-	30
JDF-2	AEN	methylammonium	OH^-	31
STA-2[a]	SAT	1,4-bisDABCO butane	OH^-	6
AlPO-GIS	GIS	dimethylammonium	F^-	32
ULM-4	–	water[b], propane-1,3-diammonium	F^-	33
AlPO-CJ2[c]	–	ammonium	OH^-, F^-	34
calcined AlPOs				
AlPO-34(calc)[d]	CHA			35
AlPO-14(calc)	AFN			36
AlPO-53(B)	AEN			37
AlPO-17(calc)	ERI			38
AlPO-18(calc)	AEI			39
STA-2(calc)	SAT			40
STA-15(calc)	SAF			41

a. Four different structural models from Ref. 6 were used for STA-2: O91O92, O92O94, O92O95 and O92O96 (see Ref. 6 and the Supporting Information (S1) for details).

b. H atoms were added manually to CSD entry XESGOS and their positions were optimized prior to the full structural optimization.

c. The optimized structure was used here in the generation of Eq. 2 and 3. For the specific discussion of AlPO-CJ2, further unoptimized and optimized structural models were investigated, as described in the text.

d. The structures determined by XRD at 110, 310 and 460 K by Amri and Walton[35] were used.

can provide a good prediction of σ_{iso}^{DFT} for the calcined AlPOs in Table 1, whereas, as shown in Figure 1, Eq. 1 yields an excellent prediction of σ_{iso}^{DFT}, with a MAE of 0.78 ppm. This small MAE confirms the ability of Eq. 1 to predict the DFT-level ^{31}P isotropic shielding (and, hence, chemical shift) to a reasonable degree of accuracy for calcined AlPOs.

As-Made AlPOs

The extension of the simple geometric prediction of σ_{iso}^{DFT} to as-made AlPOs may appear initially to be a significant challenge, owing to the presence of the SDA cations and the Al-bound anions, both of which have been demonstrated in the literature to affect the ^{31}P chemical shift.[6,21,43] The explicit parameterization of these species would be prohibitively complicated, owing to the number of permutations of anion arrangements that may occur in the third coordination shell of P (*i.e.*, P-O-Al-X, where X = O(P), OH^-, F^-) and the need to describe the size, shape, charge distribution, proximity and orientation of the SDA (and even this assumes a static structure, whereas it has been shown that motion of the SDA affects the NMR spectra of the framework atoms[11,21]). However, to a first approximation, it may be assumed that, as a consequence of the above steric and electronic factors, in as-made AlPOs, the framework will be distorted to accommodate the SDA, anions, and any dynamics present. From the point of view of the P atoms, the cumulative effects of the extraframework species will (at least to a first approximation) simply be a change in $\langle r_{PO} \rangle$ and $\langle \theta_{POAl} \rangle$. Therefore, as shown schematically in Figure 2, we will consider the influence of only the positions of the Al, O and P atoms on the ^{31}P isotropic shielding of as-made AlPOs. (This approach was demonstrated recently by Dawson *et al.*[21] for six forms of AlPO-34 with different SDAs in the pores, although in that study, experimental structures and NMR parameters were compared, rather than NMR parameters calculated from, and, therefore, corresponding exactly to, a given structure.) Figures 3(a) and (b) show that, for the as-made AlPOs in Table 1, there is a reasonable correlation between σ_{iso}^{DFT} and either $\langle r_{PO} \rangle$ or $\langle \theta_{POAl} \rangle$, although the scatter of data points about the best-fit

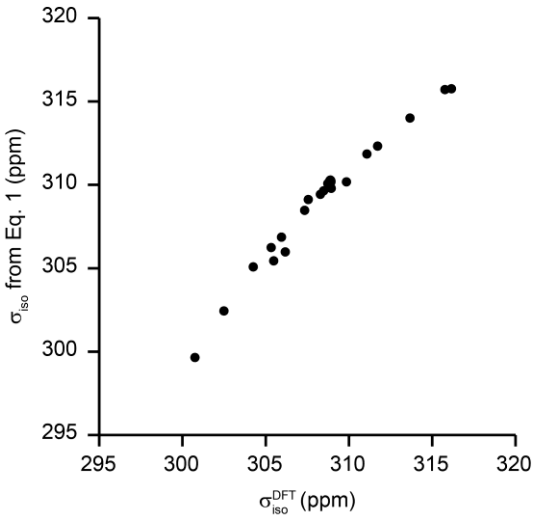

Figure 1. Plot of σ_{iso}^{DFT} against σ_{iso} (from Eq. 1) for the calcined AlPOs in Table 1.

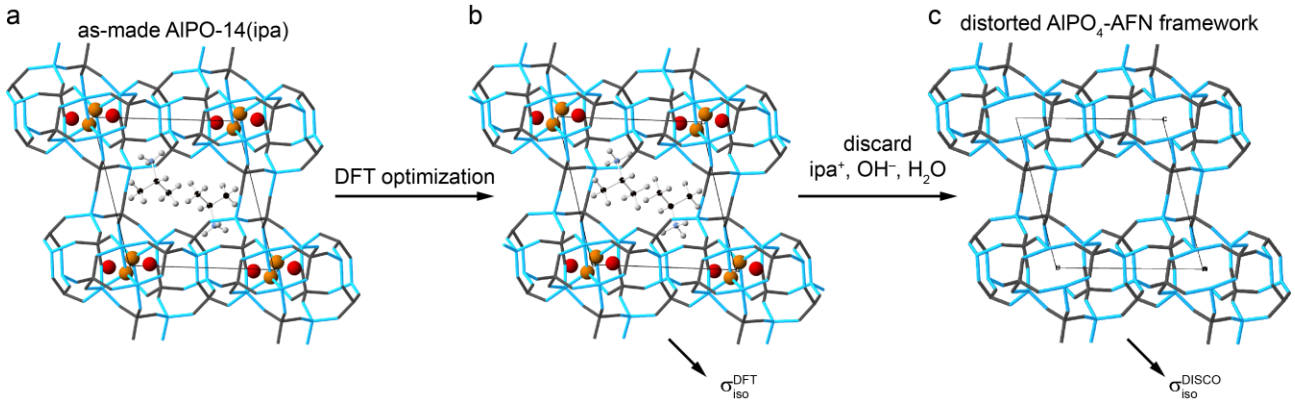

Figure 2. Example of the strategy used to consider the local structural distortions of the frameworks of ordered as-made AlPOs. (a) The experimental structure is optimized using DFT. (b) σ_{iso}^{DFT} is calculated for the optimized structure. (c) Any extraframework atoms are discarded, leaving the neutral $AlPO_4$ framework, which is not further optimized (which would give the calcined material) but left as is, so that any distortions arising from the extraframework species are retained. σ_{iso}^{DISCO} is then calculated from this structure. For unit cells containing disorder, steps (a) and (b) can be neglected.

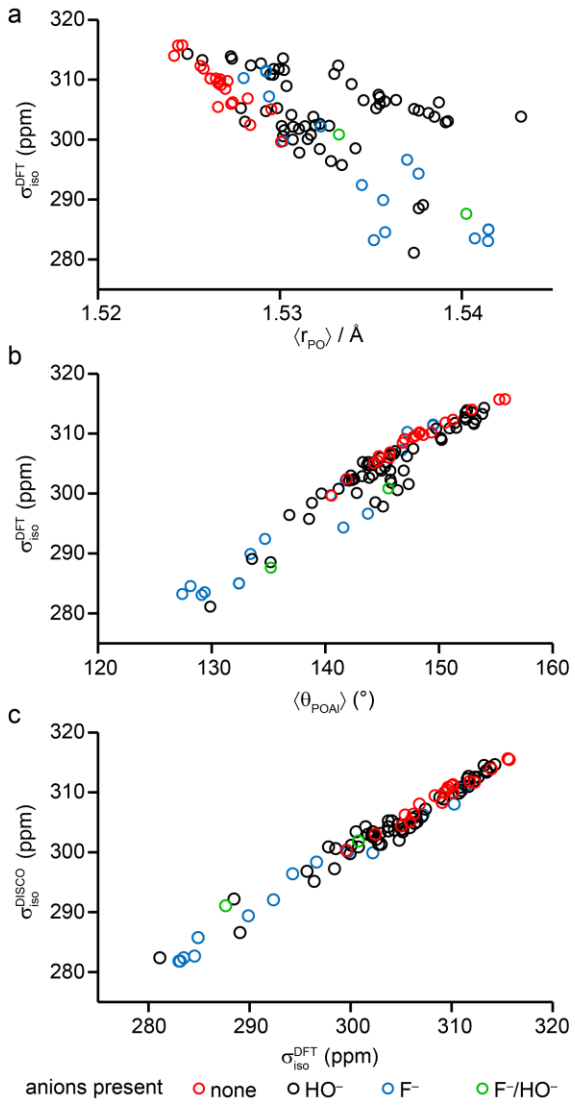

Figure 3. Plots of calculated σ_{iso}^{DFT} against (a) $\langle r_{PO} \rangle$ and (b) $\langle \theta_{POAl} \rangle$ for the AlPOs in Table 1. (c) Plot of σ_{iso}^{DISCO} against σ_{iso}^{DFT} for the AlPOs in Table 1.

lines for both structural parameters is quite high. It is important to note that the data points from fluorinated and hydroxylated AlPOs display very similar dependence on both $\langle r_{PO} \rangle$ and $\langle \theta_{POAl} \rangle$ to the points from the calcined AlPOs shown in Figure 1. However, it can be seen that the as-made materials typically sample a larger region of structure space (*i.e.*, greater ranges of both $\langle r_{PO} \rangle$ and $\langle \theta_{POAl} \rangle$) than the calcined materials. The MAE for Eq. 1 applied to the as-made AlPOs in Table 1 was 2.18 ppm, suggesting that the predictive power of the equation may be limited to the part of structure space typical of calcined AlPOs. However, it was recently shown, for analogous silicate frameworks, that one must consider the standard deviations (where the standard deviation in parameter x is denoted $\sigma(x)$, not to be confused with the isotropic shielding, denoted σ_{iso}) of r_{SiO} and θ_{SiOSi} (equivalent to r_{PO} and θ_{POAl} in AlPOs) as well as their mean values.[24] It was also demonstrated that, although the difference was relatively small, using the parameter $\cos(\langle \theta_{SiOSi} \rangle)$ gave a marginally reduced MAE (especially at higher values of θ_{SiOSi}) than using $\langle \theta_{SiOSi} \rangle$, and that, since $\langle r_{SiO} \rangle$ and $\langle r_{SiO} \rangle^2$ were effectively collinear over the relevant ranges, neglecting the $\langle r_{SiO} \rangle^2$ term was not detrimental. Therefore, a new expression for σ_{iso} for the as-made and calcined AlPOs in Table 1 was determined, giving

$$\sigma_{iso} = -105.0 \cos\left(\left\langle \theta_{POAl} \right\rangle\right) - 0.3219\,\sigma(\theta_{POAl}) - 420.4 \left\langle r_{PO} \right\rangle + 170.3\,\sigma(r_{PO}) + 862.8 \quad . \qquad (2)$$

The MAEs for Eq. 2 applied to the structures in Ref. 16 and Table 1 are summarized in Table 2, and it can be seen that, while the MAE is very low for the AlPOs studied in this work, the agreement is much poorer for the earlier set of calcined AlPOs. This is likely to arise from the fact that many of the structures in Ref. 16 were not optimized and, therefore cover a much greater range of $\langle r_{PO} \rangle$ than the optimized structures in Table 1 (1.46-1.68 Å, rather than 1.52-1.54 Å). Reintroducing the quadratic term for $\langle r_{PO} \rangle$ and redetermining the expression for σ_{iso} yields

$$\sigma_{iso} = 3313\left\langle r_{PO}\right\rangle - 1178\left\langle r_{PO}\right\rangle^2 - 15.73\,\sigma(r_{PO}) - 108.6\cos\left(\left\langle\theta_{POAl}\right\rangle\right) - 0.2799\,\sigma(\theta_{POAl}) - 2093 \quad (3)$$

which can be seen from Table 2 to give small MAEs for all as-made and calcined AlPOs considered here and in Ref. 16. Figure 3(c) shows the isotropic shielding calculated using Eq. 3 (σ_{iso}^{DISCO}, obtained from DISCO as described in the Supporting Information) plotted against σ_{iso}^{DFT} for the as-made and calcined AlPOs considered here. To gain some insight into the errors in the coefficients in Eq. 3, the 207 independent P atoms from the structures in Ref. 16 and Table 1 were distributed evenly into 23 groups and an expression of the form of Eq. 3 was calculated for each of the 33649 possible combinations of 18 of these 23 groups. Histograms showing the distribution of coefficients obtained in this manner are shown in Figure 4. As noted in recent work for silicate frameworks,[24] the constant and the coefficient for $\langle r_{PO}\rangle$ are correlated and, in this case, these are both correlated with the coefficient for $\langle r_{PO}\rangle^2$, leading to the large and non-random distribution of values obtained for Figures 4a-c. For some sets of structures (11.5% of the total number of sets), the variation in r_{PO} was negligible and no significant dependence on $\sigma(r_{PO})$ could be determined, leading to the peak at 0 in Figure 4d.

Table 2. MAEs for Eq. 1-3 for the structure sets of Ref. 16, and the calcined and as-made AlPOs in Table 1.

	MAE (ppm)		
	calcined, Ref. 16	calcined, Table 1	as made, Table 1
Eq. 1	1.60	0.78	2.18
Eq. 2	5.01	0.68	0.74
Eq. 3	1.14	0.64	1.07

From Table 2, it can be seen that, when using Eq. 3 (implemented in DISCO) to predict the ^{31}P σ_{iso} for all types of AlPO, the MAE is sufficiently small to provide experimentally-useful accuracy (given that linewidths of ^{31}P resonances for as-made AlPOs are often on the order of ~1 ppm). Indeed, perhaps the most surprising point here is that, in fact, the contributions to σ_{iso} from the SDA and framework-bound anions that cannot be represented as a structural distortion are so little.

Application to Disordered Structures

From the above results, it can be seen that it is possible to predict the ^{31}P σ_{iso} that would be calculated by DFT in both as-made and calcined AlPOs to within ~1.1 ppm, given only the P-O bond lengths and P-O-Al bond angles of the framework, neglecting any extraframework species that may be present. This ability is most immediately useful in cases where extraframework species are present but cannot accurately be located, *i.e.*, when significant spatial or temporal disorder is present. In such cases, generating an initial structural model for periodic DFT calculations can be challenging, especially when the chemical nature of the extraframework species is unknown (*e.g.*, for co-templated materials, when SDA breakdown is suspected, or during catalysis – where the guests will also be highly mobile). However, the average positions for the heavier and less mobile framework atoms can generally be determined by crystallographic diffraction and the results above suggest that these positions may be sufficient to predict σ_{iso}. In order to investigate where such a prediction is valid and where the approach is likely to break down, a series of case studies is presented below. To enable comparison of predicted and calculated σ_{iso} to experimental chemical shifts, δ_{iso}, the calculated values were referenced as described above.

Structures Containing a Disordered SDA but Ordered Anions

The organic SDAs are typically the most conformationally-flexible and dynamic components of as-made AlPOs and, to further complicate their refinement in a crystal structure, tend to contain only light elements (C, H, N, O) compared to the heavier elements in the framework. As a consequence, many SDAs are either left unrefined in crystal structures (as, most of the time, it is the calcined inorganic framework that is of ultimate practical interest), or represented by some chemically-unrealistic average conformation. In many cases,

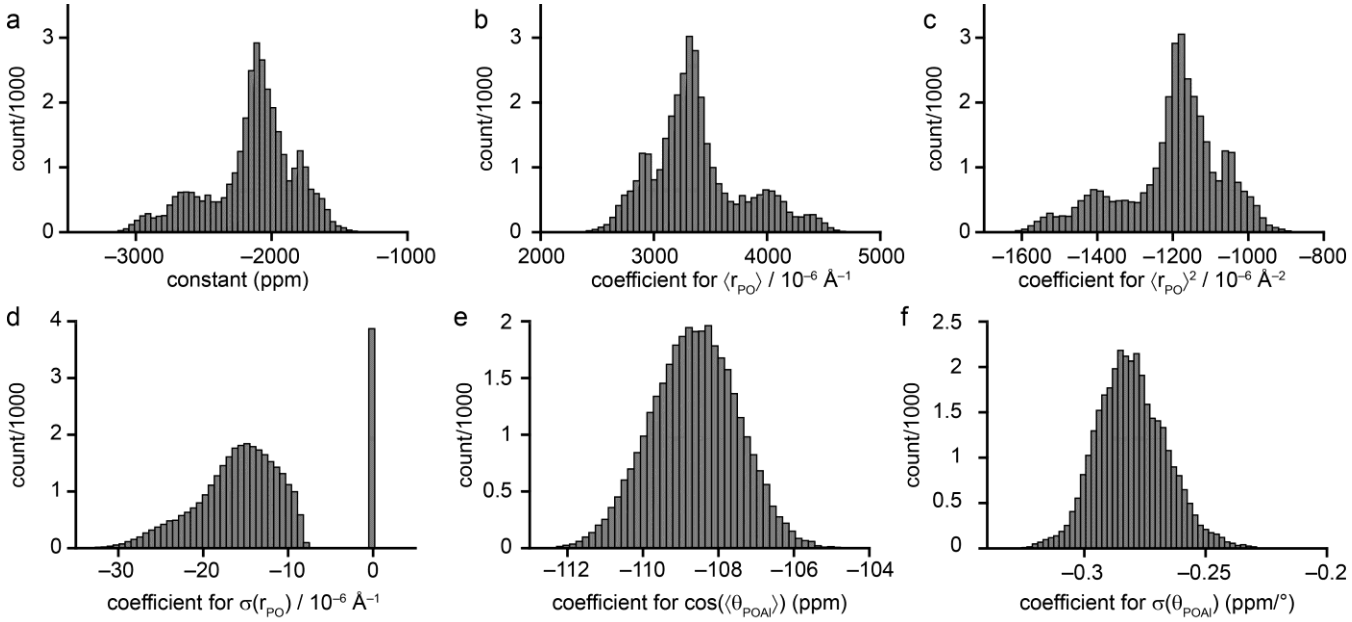

Figure 4. Plots of the distribution in coefficients for Eq. 3, obtained as described in detail in Ref. 24.

generating a starting model for DFT-based optimization can be challenging, and this often precludes the calculation of NMR parameters for a new framework. Here, three AlPOs with known framework structure, known anion locations and unknown or disordered SDAs are considered. AlPO-18(tetraethylammonium hydroxide) has the AEI framework type and a formula of $Al_6P_6O_{24}.0.98(C_2H_5)_4N.OH$, with the SDA refined at slightly below full occupancy and in two superimposed orientations, as shown in Figure 5a.[39] AlPO-21(tetramethylpropylenediamine hydroxide) has the AWO framework type but its formula has not been accurately determined as it is believed that some decomposition of the SDA to dimethylammonium and a "propyl" species may occur (C-N-C units were identified in the powder XRD (pXRD) structure, shown in Figure 5b, but the presumably more mobile "C_3" species were not located).[44] However, for comparison, other forms of AlPO-21 have been synthesized with different SDAs (dimethylamine, and N-methyl-1,3-diaminopropane) and their ^{31}P NMR spectra reported,[45,46] although their crystal structures have not been published. MDAP-2 also has the AWO framework type and was prepared with N-methyl-1,3-diaminopropane as the SDA.[46] In MDAP-2, the chosen spacegroup of the framework is such that the SDA sits on a center of symmetry and is refined in two orientations, each with 50% occupancy.

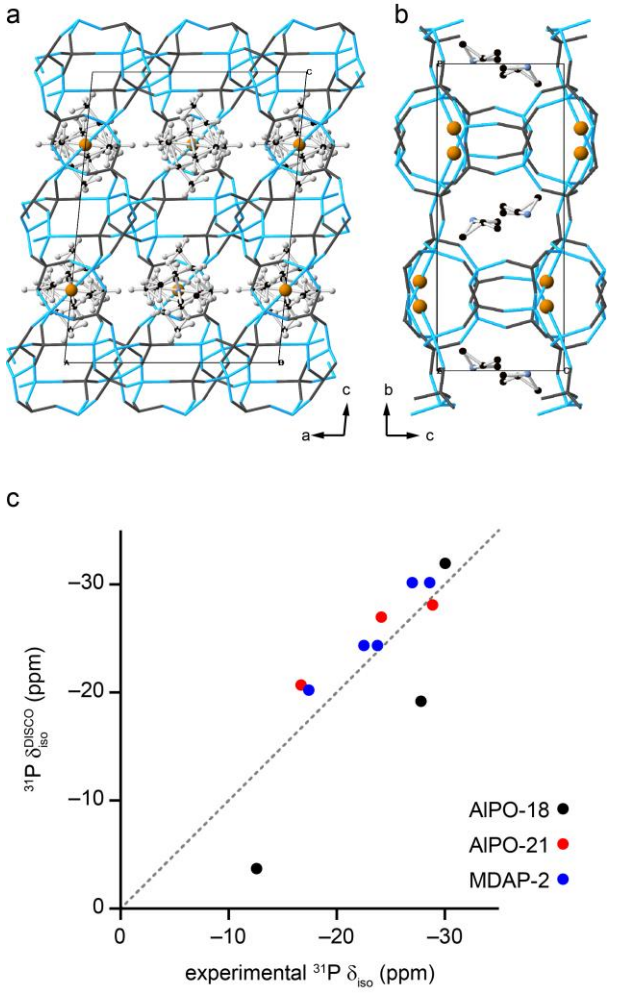

Figure 5. The published structures of (a) AlPO-18[39] and (b) AlPO-21.[44] (c) Plots of ^{31}P δ_{iso}^{DISCO} against experimental δ_{iso} for AlPO-18,[47] AlPO-21[45] and MDAP-2.[46] The broken grey line indicates the ideal 1 : 1 correspondence. In (a) and (b), blue and dark gray sticks represent Al and P, respectively. Black, blue, orange and light gray spheres represent C, N, O and H, respectively.

From the framework geometry of the published structure of AlPO-18,[39] DISCO predicts three ^{31}P resonances with δ_{iso} of –3.5, –19.0 and –31.8 ppm for P3, P1 and P2, respectively. The predicted shifts are in relatively poor agreement with the experimental values of –12.6, –28.7 and –30.1 ppm[47] (shown by the black points in Figure 5c), although this may be a reflection of the experimental accuracy in determining the O atomic coordinates, rather than a lack of predictive power of Eq. 3, since the original structure, from 1991, was solved from synchrotron pXRD.[39]

The deviation of the positions of the O atoms from an ideal tetrahedral arrangement around a P atom can be quantified using the distortion index, DI, defined as

$$DI = \frac{1}{n}\sum_{i=1}^{n}\left|\theta_{OPO(i)} - \theta_{OPO(0)}\right| , \quad (4)$$

where $\theta_{OPO(i)}$ is the ith O-P-O angle and $\theta_{OPO(0)}$ is the ideal angle (109.471° for a tetrahedron) and, for a tetrahedron, n = 6. The published structure of as-made AlPO-18 has DI values of 4.6° to 5.9°, whereas a typical range for the experimental diffraction data included in this study is 0.9° to 1.7°, with similar values for optimized structures (this is also similar to our observation for SiO_4 tetrahedra in microporous SiO_2 phases, for which DI did not exceed 2.0° on optimisation[24]). As the success of DISCO depends on reasonably accurate knowledge of the positions of the O atoms, the relatively poor match between the predicted and experimental shifts in the case of AlPO-18 is not particularly surprising.

For AlPO-21, three ^{31}P resonances are predicted from the published experimental structure, with δ_{iso} of –20.6, –26.9 and –28.0 ppm. As can be seen from the red points in Figure 5c, these predicted shifts are a reasonably good match to the experimental values reported by Liu *et al.*[45] (–16.7, –24.2 and –28.9 ppm), who used dimethylammonium as the SDA (*i.e.*, one of the species believed to be present in the AlPO-21 sample for which the structure was determined). However, the chemical shifts reported for other forms of AlPO-21 prepared with different SDAs[46,48] are in poorer agreement with these predicted values, indicating that the different SDAs can distort the framework differently. It is, therefore, possible that the "propyl" species distorts the framework differently from the dimethylammonium-only material studied by Liu *et al*. (a similar example was recently reported for AlPO-34 containing six different SDAs, where the ^{31}P δ_{iso} changed with the SDA and the majority of this variation could be ascribed to changes in the framework geometry[21]).

Tuel *et al.*[46] reported the structure and ^{31}P NMR spectrum of the AWO-type MDAP-2. The disorder of the SDA in this material causes a splitting of the two resonances at lower shift, which is not reproduced in the shifts predicted by DISCO (as there are only three crystallographically-distinct P sites in the structure). Nevertheless, the predicted values of –20.1, –24.3 and –30.1 ppm agree very well with the observed values of –17.4, –22.5, –23.8, –27.0 and –28.6 ppm (estimated from the spectrum shown in Figure 5 of Ref. 46), as shown by the blue points in Figure 5c. There is a systematic offset of ~1.6 ppm between the predicted and experimental shifts, which may

arise from the fact that there are two similar chemical shift scales for ^{31}P typically used in the literature, one of which (used in this work) takes BPO_4 as –29.6 ppm whereas the other scale takes BPO_4 as –31.2 ppm (both relative to 85% aqueous H_3PO_4),[52] and it is unclear which scale was used for the original spectroscopic data.

From the above examples, it can be seen that Eq. 3 has genuine predictive power for as-made AlPOs, even for structures where the SDA cannot be crystallographically located (and, hence, the positions of the framework atoms cannot readily be optimized by DFT). However, in order to be able to predict ^{31}P δ_{iso} in agreement with experiment, the positions of the framework atoms in the crystal structure must be a reasonable representation of the true local structure. Therefore, where there is a discrepancy between the predicted and observed NMR parameters, this may indicate that the structure contains unfeasible atomic positions (particularly for the lighter O atoms).

Structures Containing an Ordered SDA but F^-/OH^- Anion Disorder

One of the classic challenges in X-ray diffraction is the inability to distinguish between isoelectronic species, such as OH^- and F^-. In most cases, AlPOs contain either one or the other of these anionic species to balance the charge of the SDA but, in others, such as AlPO-CJ2 (with the nominal formula $AlPO_4(OH)_{0.33}F_{0.67}(NH_4)_{0.89}(H_3O)_{0.11}$), both are present.[34,43,49] This material has been comprehensively characterized by multinuclear NMR spectroscopy, which revealed a random distribution of OH^- and F^- on the anion sites.[43,50,51] The crystal structure of AlPO-CJ2 contains two P species, but the ^{31}P NMR signals from these are split, depending on the number of OH and F in the third coordination sphere of P.[34,43,49-51] The shift differences upon changing OH^- to F^- are small, on the order of ~0.5 ppm (*i.e.*, within the error margins of DISCO, however, it is unclear whether these shift differences arise from a structural effect (*i.e.*, the framework is differently distorted by the presence of OH^- or F^-), an electronic effect (*i.e.*, a difference in through-bond induction owing to the different electronegativities of O and F) or a combination of both. For the published average structure of AlPO-CJ2, DISCO predicts two ^{31}P resonances at –15.3 and –24.5 ppm, both of which are upfield from the experimental values of –10.6 and –21.4 ppm. For this published structure (without optimization), DFT calculates shifts of –11.9 and –22.6 ppm.

To estimate the electronic effects of replacing OH^- with F^-, in AlPO-CJ2, a second calculation was carried out with the H atoms of the bridging OH deleted and the O atoms replaced with F. The NMR parameters were calculated for this structure without optimization. The geometric contribution was investigated by optimizing the structural models with bridging OH and F and then recalculating their NMR parameters. Table 3 shows the values of ^{31}P δ_{iso} for both models, calculated using DFT and DISCO. It can be seen that the electronic contribution (the difference between the shifts calculated for the two unoptimized structures) is estimated to be +0.3 ppm for P2 and negligible for P1. The combined geometric and electronic contribution (the difference between the shifts of the two optimized structures) is estimated to be –0.5 ppm for P1 and –2.3 ppm for P2. From these values, the geometric contribution (*i.e.*, the shift differences arising from different framework distortions when the different anions are present) can be estimated to be –0.8 ppm for P1 and –2.3 ppm for P2. In principle, since the majority of the shift differences occurring on substituting F^- for OH^- arise from a geometric effect, it is anticipated that DISCO should be able to be predict these well. Indeed, as can be seen from Table 3, the shift differences predicted by DISCO for the optimized structures are –0.8 ppm for P1 and –1.7 ppm for P2 (*cf.* the MAEs in Table 2). Therefore, it is possible to use DISCO to assign the resonances in the experimental ^{31}P NMR spectrum of AlPO-CJ2 not just to P1 or P2 species, but also to P1(OH)/P1(F) and P2(OH)/P2(F) species.

Table 3. ^{31}P δ_{iso} calculated by DFT and DISCO for models of AlPO-CJ2 with bridging OH or F, before and after optimization.

Structure	DFT δ_{iso} (ppm)		δ_{iso}^{DISCO} (ppm)	
	P1	P2	P1	P2
OH, unoptimized	–22.6	–11.9	–24.5	–15.3
F, unoptimized	–22.3	–11.9	–24.5	–15.3
OH, optimized	–22.9	–11.4	–23.6	–14.3
F, optimized	–23.4	–13.7	–24.4	–16.0

Structures with Partially-Occupied Anions

A more extreme example of anion disorder is where the anion sites are only partially occupied, leading to an Al site that may be either Al^{IV} or $Al^{V/VI}$ in the second coordination sphere of P. The crystallographically-determined structures of such materials typically have a framework geometry comprising a weighted average of the atomic positions for the different coordination stated of Al.

AlPO-17 (containing piperidine as the SDA)[53] and AlPO-ERI[54] (with N,N,N′,N′-tetramethyl-1,6-diaminohexane (TMHDA) as the SDA) both have the erionite (ERI) structure type, with a formula of $Al_{18}P_{18}O_{72}$.nSDA.4OH (where n = 4 for AlPO-17 and n = 2 for AlPO-ERI). The structure of AlPO-17 was determined by Pluth *et al.*, who were unable to distinguish between C and N atoms or locate any of the H atoms of the pyridinium cations.[53] The structure could, therefore, be refined in the $P6_3/m$ space group, which gives rise to two distinct P and Al sites. However, this structure contains three equivalent anion sites in each of the cancrinite cages but, for charge balancing purposes, these must only be 2/3 occupied. The ^{31}P spectrum predicted by DISCO from this structure would contain two resonances at –28.3 and –31.5 ppm in a 1 : 2 intensity ratio (neither of which is particularly close to the reported experimental value of –24.2 ppm[3]). As discussed above, this discrepancy is not particularly surprising, given that the anion sites are only partially occupied and the average bond geometry around the crystallographic P sites is, therefore, not a true representation of the bond geometry around any one given P atom. The TMHDA in AlPO-ERI was more readily located by Tuel *et al*., allowing the structure to be refined in the lower-symmetry $P2_1$ space group.[54] This yielded a structure containing 9 inequivalent P and Al sites, and, although the cancrinite cages still contained three anion sites (as shown in Figure 6a, one of these was refined as fully occupied whereas the other two were refined as each having 1/2 occupancy. Tuel *et al.* also reported the ^{31}P NMR spectrum of AlPO-ERI, which contained seven resonances with δ_{iso} of –17.3,–18.9, –21.6, –23.5, –25.5, –27.4 and –30.8 ppm and relative integrated

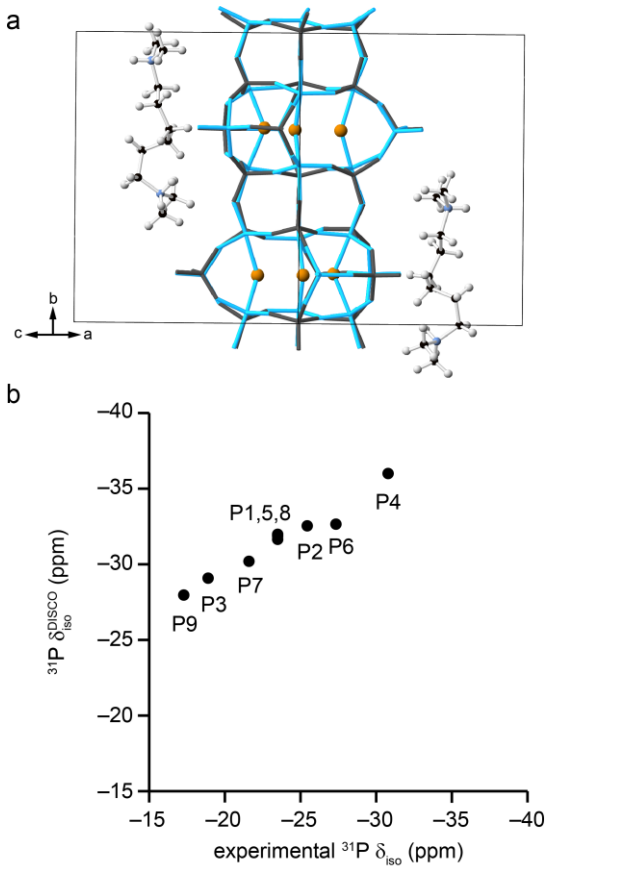

Figure 6. (a) The structure of AlPO-ERI,[54] containing three anion sites per cancrinite cage, each with 2/3 occupancy. Blue and dark gray sticks represent Al and P, respectively. Black, blue, orange and light gray spheres represent C, N, O and H, respectively. (b) Plot of ^{31}P δ_{iso}^{DISCO} against experimental δ_{iso}[54] for AlPO-ERI.

intensities of 1 : 1 : 1 : 3 : 1 : 1 : 1.[53] As shown in Figure 6b, the ^{31}P peak positions predicted from the structure of AlPO-ERI are in reasonably good agreement with the experiment, although the predicted shift range of 8.1 ppm is much smaller than the experimental range of 13.5 ppm. Despite the use of multinuclear and multidimensional NMR experiments, Tuel *et al.* could not provide a complete spectral assignment, owing to the disordered nature of the material. Based on their published structure, we can now suggest the assignment indicated in Figure 6b, although it should be noted that the fractional occupancy gives rise to an average diffraction structure with contributions from local structures containing different combinations of occupied and vacant anion sites. This change in the precise Al coordination state at the local level will alter the local bonding geometry and, again, one should not expect the average crystal structure to be an accurate representation of the local geometry at any given P atom. This is reflected in the relatively high DI values observed for this structure, of up to 3.8° for P5.

A similar case was also reported for STA-2,[6,55] which has the SAT framework type and a formula of $Al_{12}P_{12}O_{48}$.BDAB.2OH (BDAB = 1,4-bisDABCO butane) for its as-made form. The structure of STA-2, shown in Figure 7a, also contains cancrinite cages, in which the three anion sites are located. However, to balance the charge of the BDAB (present as a dication), the anion sites must be only 1/3

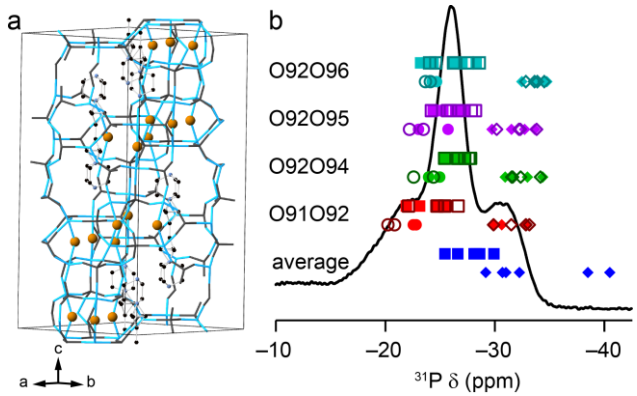

Figure 7. (a) The structure of STA-2,[6] containing three anion sites per cancrinite cage, each with 1/3 occupancy. Blue and dark gray sticks represent Al and P, respectively. Black, blue, and orange spheres represent C, N and O, respectively. H are omitted for clarity. (b) ^{31}P (14.1 T, 14 kHz MAS) NMR spectrum of STA-2 (black line) and δ_{iso} obtained from DISCO (filled points) or DFT (open points) for four structural models with localized anions (see Ref. 6 for details) or the crystallographic average structure[6,55] (dark blue points, DISCO predictions only). Diamonds indicate P1 species, squares P2 and circles P1* (P1 and P1* are not distinct in the average structure in Ref. 6) *N.B.*, this spectrum was referenced to 85% H_3PO_4 with B**P**O_4 at –29.6 ppm, as opposed to the –31.2 ppm for B**P**O_4 used in Ref. 6.

occupied. Seymour *et al.*[6] generated a series of structural models, some of which had two anions in one cage and the next cage empty, and others which had one anion per cage, and optimized these with DFT (see Ref. 6 for further details). The ^{31}P NMR spectrum of as-made STA-2, shown in Figure 7b, contains three broad resonances, at approximately –22, –26 and –31 ppm (note that these differ from the shifts reported by Seymour *et al.*, who used BPO_4 at –31.2 ppm as the reference, rather than the –29.6 ppm used throughout the present work).[6] On the basis of the computed shifts and ^{27}Al-^{31}P correlation experiments, these resonances could be assigned to P sites in the 6-membered rings (6mr) connected to two Al bridged by the same anion to form a three-membered ring (P1*, –22 ppm), the same P sites without the bridging anion (P1, –31 ppm), or P sites in the double 6-membered ring (d6r) with any arrangement of nearby anions (P2, –26 ppm) – examples of these local geometries are shown in the Supporting Information (S1). The ^{31}P δ_{iso} values predicted for the experimental average structure[6] are shown overlaid with the experimental spectrum in Figure 7b (dark blue points) and, as expected, the agreement between observed and calculated shifts is poor. Figure 7b also shows the ^{31}P δ_{iso} predicted for four of the structural models investigated by Seymour *et al.*[6] These models have all atoms located and fully occupied, allowing NMR parameters to be calculated by DFT (open points) as well as by DISCO (filled points). The results from the DFT calculations were described in detail by Seymour *et al.*[6] and, here, we wish only to highlight that the DISCO predictions agree very well with the DFT values (MAE of 0.81 ppm for the four models) considered.

The maximum DI value for the P sites in the (optimized) structural models of STA-2 was 2.7° (*cf.* the range of 2.5-6.9° for the average structure of Castro *et al.*[55]) suggesting that these are perhaps more reasonable representations of the local

structure around the P atoms than were found in the structure of AlPO-ERI above. This again highlights the different sensitivities of crystallographic diffraction and NMR spectroscopy to different lengthscales. The averaged structure presented by diffraction clearly cannot accurately describe the local environment of any one P atom in the material and, therefore, it is meaningless to attempt to predict NMR parameters directly from this. In cases where local structural models can be determined and their geometry optimized, it is possible to predict more useful values but, in such cases, the DFT calculations of NMR parameters may represent a minimal additional computational expense on top of the cost of the optimization.

Extensively Disordered Structures

It is often the case that, when a crystallographic structure solution is particularly challenging, even the most careful analysis of the data will lead to an incomplete picture of the material. One such example is the structure of STA-15(tetrapropylammonium hydroxide),[41] for which a synchrotron pXRD pattern was recorded, but neither the N atoms of the SDA nor the OH^- anions could be located. It is, therefore, challenging to generate a potential structural model for DFT calculations in this case since, unlike the cases above, there is not even an indication of where the anions (or, indeed, the cations) may be located. DISCO predicts that the four P sites in the refined structure of as-made STA-15 would have shifts of –30.0, –30.4, –31.8 and –32.0 ppm, which, given the extensive disorder in the structure, is in remarkably good agreement with the single resonance between *ca*. –26 and –32 ppm observed experimentally. Han *et al*.[41] assigned a broader downfield resonance in the experimental spectrum to P-O-$Al^{V/VI}$ species, which is not predicted by DISCO, as the published structural model does not contain any anions.

Hydrated AlPOs

Upon calcination, many AlPO frameworks can adsorb atmospheric water. These calcined, hydrated AlPOs contain only neutral extraframework water, although this can still coordinate to the framework to give $Al^{V/VI}$. Here, we use AlPO-34 (CHA-type framework) as a model system, which has two hydrated states that have been characterized by both XRD and solid-state NMR spectroscopy by Tuel and co-workers.[56,57] The two hydrated states of AlPO-34 have the same framework connectivity but different numbers of H_2O molecules per formula unit.[56,57] Form A has the unit cell formula $Al_6P_6P_{14}.11H_2O$, whereas form B has the formula $Al_6P_6P_{14}.12H_2O$. For form B, on the basis of a ^{27}Al-^{31}P correlation experiment and the structure-spectrum relationship of Müller *et al.*,[9] Tuel *et al.*[56] assigned the ^{31}P NMR spectrum as summarized in Table 4. From the published structure, DISCO predicts ^{31}P δ_{iso} in poor agreement with experiment (MAE of 5.2 ppm), as shown in Table 4. This poor agreement possibly arises because, as is frequently observed for structures derived from Bragg diffraction methods, the DI values are quite high. In this case, P1-P5 have DI of 2.8-3.8°, whereas P6 has a more realistic DI of 1.5° and the predicted shift for this P site is 0.1 ppm away from the experimental value. Poulet *et al.* subsequently used DFT to optimize several structural models of hydrated AlPO-34 form B with different starting positions for H atoms, and reported coordinates for the lowest-energy structure (0_{final} in their notation).[57] The 0_{final} structure has reduced DI for all P sites, with only P2 and P3 having DI > 2.0°. DISCO predicts the shifts given in Table 4, now with a reduced MAE of 2.4 ppm with respect to the experimental values. However, Poulet *et al.* also investigated the time-dependent nature of the structure using molecular dynamics (MD) calculations, and showed that over the 3 ps run at a temperature of 300 K, the positions of some of the water molecules were highly variable.[57] It is, therefore, perhaps unsurprising that neither the time- and length-averaged experimental structure (at 283 K) and the static (0 K) optimized structure provide a very accurate prediction of the experimental NMR spectrum (at ~300 K). Indeed, as shown in the Supporting Information (S3), form B of hydrated AlPO-34 exhibits significant variation in the positions of the ^{31}P resonances as a function of temperature (even below the temperature of the transition to form A), confirming the dynamic nature of this material. The case of hydrated AlPOs may, therefore, be seen as an extension to the case of partially-occupied anion sites described above. In, *e.g.*, AlPO-17, AlPO-ERI and STA-2, the local environment of P could be reasonably well modeled simply by a series of static snapshots of the structure, with the anions localized. However, the MD calculations of Poulet *et al.*[57] indicate that, in the presence of framework-bound water, the coordination state of any one Al in hydrated AlPOs may vary significantly over time, meaning that a more dynamic picture of the structure may be necessary. In the 2.5 ps of motion simulated by Poulet *et al.*,[57] 5000 structures were generated, and each one of these will have some contribution to the observed ^{31}P chemical shifts. Clearly, such a large number of DFT-level calculations would be extremely time consuming but, as discussed below, it would be entirely feasible to predict the outcome of such a large volume of calculations using DISCO.

Table 4. ^{31}P δ_{iso} observed experimentally[56] (exp.) and predicted by DISCO for structural models of AlPO-34 hydrated form B, from pXRD[56] and optimized by DFT.[57]

	exp. δ_{iso} (ppm)[56]	δ_{iso}^{DISCO} (ppm)	
		XRD structure[56]	0_{final}[57]
P1	–21.0	–31.4	–23.2
P2	–24.3	–32.4	–23.5
P3	–26.2	–22.9	–21.4
P4	–26.2	–36.0	–27.3
P5	–28.2	–34.8	–25.5
P6	–22.5	–22.6	–20.0

Performance and Applicability of DISCO

As DISCO is a geometry-based rather than quantum-mechanical code, calculation times are very rapid – typically on the order of tens of ms (see the Supporting Information (S4) for more details). This indicates that DISCO could readily be applied to very large systems (*e.g.*, supercells used to model disorder), where even the approximate prediction of NMR parameters may provide a valuable link between the structure and the NMR spectra of such disordered systems. The ability to rapidly determine approximate NMR parameters for many hundreds or thousands of atoms means that one potential application of DISCO could be to generate NMR parameters from the results of MD calculations. Such calculations determine the evolution (or trajectory) of a system over time periods on the order of ps to ns (depending on the level of theory used and available computing power). The output of an MD calculation is a series of structures, corresponding to the individual time increments in the trajectory. Typically, in order to model motion of, *e.g.*, a guest

molecule within the pores of zeolitic materials, a relatively large supercell of the parent crystal structure is used, meaning that the output from an MD calculation contains (typically) thousands of structures, each containing hundreds or thousands of atoms. Calculating NMR parameters for all of these structures using DFT would be impractical, and is unlikely ever to be a reasonable prospect with conventional computing technology (particularly as the size of MD output will be likely to scale more rapidly with computing power than the capability to carry out the ever larger number of corresponding higher-level DFT calculations of the NMR parameters). However, if DISCO can be used to reduce the calculation time for the NMR parameters to the timescale of a few milliseconds per structure, then calculating the NMR parameters for every structure in even a very large MD run would be feasible. This approach could provide a direct (although approximate) link between the MD simulation of, *e.g.*, a dynamic process occurring within the pores of an AlPO, and experimental NMR characterization of the same system. Dynamic effects are frequently observed in as-made, calcined and hydrated AlPOs, and it can be envisaged that such a link would also allow for the investigation of possible catalytic reaction mechanisms, or of host-guest interactions in applications such as gas separation and drug delivery.

Cuny *et al.* recently demonstrated a similar approach, termed NN-NMR, based on the use of neural networks to predict the DFT-level ^{17}O and ^{29}Si NMR parameters of silicates, and also proposed that the methodology would be suitable for investigating very large, amorphous, or dynamic materials,[59] It seems, therefore, that the future of DFT calculations of NMR parameters in materials science might be as a benchmark for more restricted (in terms of the materials to which they can be applied) predictive algorithms, with these algorithms then being used to predict the NMR spectra arising from ever larger and more complex structures. It remains to be seen, however, whether the approaches such as NN-NMR, which presents even more of an inscrutable "black box" method than DFT, or those such as DISCO, which present a clearer link between structure and spectrum, find wider acceptance in the long term.

Conclusions

We have demonstrated a simple structure-spectrum relationship for predicting the ^{31}P isotropic chemical shifts that would be calculated by a typical periodic planewave DFT approach, for as-made and calcined AlPOs. This relationship has the advantage that it does not require the positions of all atoms to be known in cases of disorder of the guest species (SDAs, water, *etc.*), as the effects of these species manifest as a change in the local framework geometry. This allows the possibility to predict the outcome of a DFT calculation (with a typical accuracy of ~1.1 ppm), even when it would be impossible or very challenging to run the actual DFT calculation. While some overparameterisation is inevitable with such a simple approach, which aims to ascribe all changes in the ^{31}P chemical shift to variation in just two parameters, this is still likely to be of great interest in cases where a system is dynamic and with guest species that are changing over time (*e.g.*, in most AlPO structures, and particularly reactions catalyzed by AlPOs). A second advantage of our method is that it is based purely on geometry, rather than quantum mechanics and the predictions are, therefore, around five orders of magnitude more rapid than DFT calculations.

We presented several case studies to test the application of out structure-spectrum relationship to real experimental data on more complex systems. These demonstrated that, in some cases, the time- and space-averaged structures determined by crystallographic diffraction are poor representations of the local bonding environment of P sites, with unfeasibly large and small O-P-O bond angles leading to large distortion indices. As the ^{31}P chemical shift is very sensitive to small changes in the local geometry, it was often not possible to use the experimental crystal structures to predict meaningful chemical shifts (for our approach or any similar method that relies on accurate knowledge of the structure). This phenomenon is well known within the field of solid-state NMR spectroscopy, with many researchers now routinely optimizing crystal structures computationally prior to the calculation of NMR parameters. While the aim of our structure-spectrum relationship is to predict NMR parameters where these cannot be calculated by a higher level of theory (thus precluding the use of such computational pre-optimization of the structure), there remains the inescapable fact that, in order to provide a meaningful prediction, the structure itself must be a meaningful representation of the material. In cases where such structures were available, we demonstrated that the structure-spectrum relationship does have genuine predictive power. Although not demonstrated here, it would also be possible to predict ^{31}P chemical shifts for partial structures if they could be optimized using a lower level of theory to achieve a more realistic geometry.

Unfortunately, it would appear that cases where a simple, static crystal structure of an AlPO can be seen as an accurate representation of the structure experienced by the ^{31}P nuclei may be quite scarce. Many AlPOs contain disorder and dynamics on timescales from ps to days,[21,35,38,42,57,58,60] and more detailed modeling of these features will require either large static supercell calculations, or even larger molecular dynamics simulations. Using DFT to calculate the NMR parameters from the outputs of such calculations is likely to remain unappealingly costly for the foreseeable future. Therefore, while we do not believe that our approach will ever supersede DFT calculations where such are possible, the high speed and reasonable accuracy of our approach means that it is likely to find application in cases where DFT-level calculations are desirable, but are simply not feasible. In light of these possible applications, we also present DISCO – a code written in FORTRAN90 to carry out calculation of the structural and NMR parameters from a given set of atomic coordinates. To facilitate its use alongside MD calculations, DISCO has the ability to operate in batch mode, with the submission of a list of input files, and can achieve very high throughput, such that the calculation of the NMR parameters for every step of a MD simulation is expected to take on the order of minutes. We envisage that the ability of DISCO to provide a rapid and reasonably accurate link between a theoretical model of a disordered or dynamic AlPO-based system will have applications in *e.g.*, modelling gas storage and separation, drug delivery and catalytic pathways.

ASSOCIATED CONTENT

Supporting Information

Further information on the structures and structural models used, higher-precision values of the coefficients in the equations, variable-temperature ^{31}P NMR spectra of calcined, rehydrated AlPO-34, the DISCO user guide, source code and example input files are provided in the Supporting Information. The Supporting Information is available free of charge on the ACS Publications website.

AUTHOR INFORMATION

Corresponding Author

*email: dmd7@st-andrews.ac.uk, sema@st-andrews.ac.uk

ACKNOWLEDGMENTS

SEA would like to thank EPSRC for computational support through the Collaborative Computational Project on NMR Crystallography (CCP-NC), *via* EP/M022501/1), the Leverhulme Trust (F/00 268/BJ) and the Royal Society and the Wolfson Foundation for a merit award. Dr David McKay is thanked for improving the DISCO compilation process. The research data (and/or materials) supporting this publication can be accessed at DOI: XXX.

REFERENCES

1. Wilson, S. T.; Lok, B. M.; Messina, C. A.; Cannan, T. R.; Flannigen, E. M. Aluminophosphate Molecular Sieves: A New Class of Microporous Crystalline Inorganic Solids. *J. Am. Chem. Soc.*, **1982**, *104*, 1146–1147.

2. Wright, P. A. *Microporous Framework Solids*, **2008**, Royal Society of Chemistry, Cambridge, UK.

3. Blackwell, C. S.; Patton, R. L.; Aluminum-27 and Phosphorus-31 Nuclear Magnetic Resonance Studies of Aluminophosphate Molecular Sieves. *J. Phys. Chem.*, **1984**, *88*, 6135–6139.

4. Ashbrook, S. E.; Dawson, D. M.; Seymour, V. R. Recent Developments in Solid-State NMR Spectroscopy of Crystalline Microporous Materials. *Phys. Chem. Chem. Phys.*, **2014**, *16*. 8223–8242.

5. Philippou, A.; Salehirad, F.; Luigi, D.-P.; Anderson, M. W. ^{31}P Magic-Angle-Turning NMR Studies of the Chemical and Electronic Nature of Phosphorus in Magnesium Aluminophosphate MgAPO-20. *J. Phys. Chem. B*, **1998**, *102*, 8974–8977.

6. Seymour, V. R.; Eschenroeder, E. C. V.; Castro, M.; Wright, P. A.; Ashbrook, S. E. Application of NMR Crystallography to the Determination of the Mechanism of Charge-Balancing in Organocation-Templated AlPO STA-2. *CrystEngComm*, **2013**, *15*, 8668–8679.

7. Seymour, V. R.; Eschenroeder, E. C. V.; Wright, P. A.; Ashbrook, S. E. An NMR Crystallographic Approach to Monitoring Cation Substitution in the Aluminophosphate STA-2. *Solid State Nucl. Magn. Reson.*, **2015**, *65*, 64–74.

8. Moran, R. F.; Dawson, D. M.; Ashbrook, S. E. Exploiting NMR Spectroscopy for the Study of Disorder in Solids. *Int. Rev. Phys. Chem.*, **2017**, *36*, 39–115.

9. Müller, D.; Jahn, E.; Ladwig, G.; Haubenreisser, U. High-Resolution Solid-State ^{27}A1 and ^{31}P NMR: Correlation between Chemical Shift and Mean Al-O-P Angle in $AlPO_4$ Polymorphs. *Chem. Phys. Lett.*, **1984**, *109*, 332–336.

10. Kanehashi, K.; Nemoto, T.; Saito, K. Through-Bond and Through-Space Connectivities of Amorphous Aluminophosphate by Two-Dimensional ^{27}Al–^{31}P Heteronuclear NMR. *J. Non-Cryst. Solids*, **2007**, *353*, 4227–4231.

11. Ashbrook, S. E.; Cutajar, M.; Pickard, C. J.; Walton, R. I.; Wimperis, S. Structure and NMR Assignment in Calcined and As-Synthesized Forms of AlPO-14: a Combined Study by First-Principles Calculations and High-Resolution ^{27}Al-^{31}P MAS NMR Correlation. *Phys. Chem. Chem. Phys.*, **2008**, *10*, 5754–5764.

12. Ashbrook, S. E.; Dawson, D. M.; Exploiting Periodic First-Principles Calculations in NMR Spectroscopy of Disordered Solids. *Acc. Chem. Res.*, **2013**, *46*, 1964–1974.

13. Sneddon, S.; Dawson, D. M.; Pickard, C. J.; Ashbrook, S. E. Calculating NMR Parameters in Aluminophosphates: Evaluation of Dispersion Correction Schemes. *Phys. Chem. Chem. Phys.*, **2014**, *16*, 2660–2673.

14 Ashbrook, S. E.; McKay, D. Combining Solid-State NMR Spectroscopy with First Principles Calculations – a Guide to NMR Crystallography. *Chem. Commun.*, **2016**, *52*, 7186–7204.

15. Clark, S. J.; Segall, M. D.; Pickard, C. J.; Hasnip, P. J.; Probert, M. J.; Refson, K.; Payne, M. C. First Principles Methods using CASTEP. *Z. Kristallogr.*, **2005**, *220*, 567–570.

16. Dawson, D. M.; Ashbrook, S. E. Investigating Relationships between the Crystal Structure and ^{31}P Isotropic Chemical Shifts in Calcined Aluminophosphates. *J. Phys. Chem. C*, **2014**, *118*, 23285–23296.

17. Pickard, C. J.; Mauri, F. All-Electron Magnetic Response with Pseudopotentials: NMR Chemical Shifts. *Phys. Rev. B*, **2001**, *63*, 245101.

18. Yates, J. R.; Pickard, C. J.; Mauri, F. Calculation of NMR Chemical Shifts for Extended Systems using Ultrasoft Pseudopotentials. *Phys. Rev. B*, **2007**, *76*, 024401.

19. Tkatchenko, A.; Scheffler, M. Accurate Molecular van der Waals Interactions from Ground-State Electron Density and Free-Atom Reference Data. *Phys. Rev. Lett,*. **2009**, *102*, 073005.

20. McNellis, E. R.; Meyer, J.; Reuter, K. Azobenzene at Coinage Metal Surfaces: Role of Dispersive van der Waals Interactions. *Phys. Rev. B*, **2009**, *80*, 205414.

21. Dawson, D. M.; Griffin, J. M.; Seymour, V. R.; Wheatley, P. S.; Amri, M.; Kurkiewicz, T.; Guillou, N.; Wimperis, S.; Walton, R. I.; Ashbrook, S. E. A Multinuclear NMR Study of Six Forms of AlPO-34: Structure and Motional Broadening. *J. Phys. Chem. C*, **2017**, *121*, 1781–1793.

22. Dawson, D. M. *PhD. Thesis* **2014**, University of St Andrews, St Andrews, UK.

23. MATLAB and Statistics Toolbox Release 2011b, The MathWorks, Inc., Natick, MA.

24. Dawson, D. M.; Moran, R. F.; Ashbrook, S. E. An NMR Crystallographic Investigation of the Relationships between the Crystal Structure and ^{29}Si Isotropic Chemical Shift in Silica Zeolites. *J. Phys. Chem. C*, **2017**, *121*, 15198–15210.

25. Baerlocher, C.; McCusker, L. B. Database of Zeolite Structures. http://www.iza-structure.org/databases/

26. Cooper, E. R.; Andrews, C. D.; Wheatley, P. S.; Webb, P. B.; Wormald, P and Morris, R. E.; Ionic Liquids and Eutectic Mixtures as Solvent and Template in Synthesis of Zeolite Analogues. *Nature*, **2004**, *430*, 1012–1016.

27. Parnham, E. R. and Morris, R. E. 1-Alkyl-3-Methyl Imidazolium Bromide Ionic Liquids in the Ionothermal Synthesis of Aluminium Phosphate Molecular Sieves. *Chem. Mater.*, **2006**, *18*, 4882–4887.

28. Harding, M. M.; Kariuki, B. M. Microcrystal Structure Determination of $AlPO_4$-CHA using Synchrotron Radiation. *Acta Cryst.*, **1994**, *50*, 852–854.

29. Aubert, E.; Porcher, F.; Souchassou, M.; Lecomte, C. Characterization of Intra-Framework and Guest/Host Interactions in the $AlPO_4$-15 Molecular Sieve by Charge-Density Analysis. *Acta. Cryst.*, **2003**, *B59*, 687–700.

30. Broach, R. W.; Wilson, S. T.; Kirchner, R. M. Corrected Crystallographic Tables and Figure for As-Synthesized $AlPO_4$-14. *Micropor. Mesopor. Mater.*, **2003**, *57*, 211–214.

31. Chippindale, A. M.; Powell, A. V.; Jones, R. H.; Thomas, J. M.; Cheetham, A. K.; Huo, Q.; Xu, R. A 3-Dimensional Framework Aluminophosphate $(CH_3NH_3)^+[Al_3P_3O_{13}H]^-$ *Acta Crys.*, **1994**, *C50*, 1537–1540.

32. Paillaud, J.-L.; Marichal, C.; Roux, M.; Baerlocher, C.; Chézeau, J. M. Tripling of the Unit Cell Volume of the Non-Centrosymmetric $AlPO_4$-SOD after Dehydration: a Structural Study of a Reversible Process. *J. Phys. Chem. B*, **2005**, *109*, 11893–11899.

33. Simon, N.; Marrot, J.; Loiseau, T.; Férey, G. Hydrothermal Synthesis and Crystal Structures of Two Open-Framework

Fluorinated Aluminum Phosphates Templated by 1,3-Diaminopropane (ULM-4 & MIL-64). *Solid State Sci.*, **2006**, *8*, 1361–1367.
34. Férey, G.; Loiseau, T.; Lacorre, P.; Taulelle, F. Oxyfluorinated Microporous Compounds. I. Crystal Structure of $(NH_4)_{0.93}(H_3O)_{0.07}GaPO_4(OH)_{0.5}F_{0.5}$; Reexamination of the Structure of $AlPO_4$-CJ2. *J. Solid State Chem.*, **1993**, *105*, 179–190.
35. Amri, M.; Walton, R. I. Negative Thermal Expansion in the Aluminum and Gallium Phosphate Zeotypes with CHA and AEI Structure types. *Chem. Mater.*, **2009**, *21*, 3380–3390.
36. Broach, R. W.; Wilson, S. T.; Kirchner, R. M. Synthesis and Structures of As-Synthesized and Calcined $AlPO_4$-14 Revealing a Three-Dimensional Channel System with 8-Ring Pores. in *Proceedings of the 12th International Zeolite Conference*, Eds. Treacy, M. M. J; Marcus, B. C.; Bisher, M. E.; Higgins, J. B. Materials Research Society, Warrendale, PA., Vol. III, 1998, pp.1715–17 22.
37. Kirchner, R. M.; Grosse-Kunstleve, R. W.; Pluth, J. J.; Wilson, S. T.; Broach R. W.; Smith, J. V. The Structures of As-Synthesized $AlPO_4$-53(A), Calcined Dehydrated $AlPO_4$-53(B), and $AlPO_4$-53(C), a New Phase Determined by the FOCUS Method. *Micropor. Mesopor. Mater.*, **2000**, *39*, 319–332.
38. Attfield; M. P.; Sleight, A. W. Exceptional Negative Thermal Expansion in $AlPO_4$-17. *Chem. Mater.*, **1998**, *10*, 2013–2019.
39. Simmen, A.; McCusker, L. B.; Baerlocher, C.; Meier, W. M. The Structure Determination and Rietveld Refinement of the Aluminophosphate $AlPO_4$-18. *Zeolites*, **1991**, *11*, 654–661.
40. Noble, G. W.; Wright, P. A.; Kvick, A. The Templated Synthesis and Structure Determination by Synchrotron Microcrystal Diffraction of the Novel Small Pore Magnesium Aluminophosphate STA-2. *J. Chem. Soc., Dalton. Trans.*, **1997**, 4485–4490.
41. Han, Z.; Picone, A. L.; Slawin, A. M. Z.; Seymour, V. R.; Ashbrook, S. E.; Zhou, W.; Thompson, S. P.; Parker, J. E.; Wright, P. A. Novel Large-Pore Aluminophosphate Molecular Sieve STA-15 Prepared Using the Tetrapropylammonium Cation As a Structure Directing Agent. *Chem. Mater.*, **2010**, *22*, 338–346.
42. Ashbrook, S. E.; Cutajar, M.; Griffin, J. M.; Lethbridge, Z. A. D.; Walton, R. I.; Wimperis, S. Transformation of AlPO-53 to JDF-2: Reversible Dehydration of a Templated Aluminophosphate Studied by MAS NMR and Diffraction. *J. Phys. Chem. C*, **2009**, *113*, 10780–10789.
43. Martineau, C.; Mellot-Draznieks, C.; Taulelle, F. NMR crystallography of $AlPO_4$-CJ2: from the topological network to the local (OH)/F distribution *Phys. Chem. Chem. Phys.*, **2011**, *13*, 18078–18087.
44. Bennett, J. M.; Cohen, J. M.; Artioli, G.; Pluth, J. J.; Smith, J. V. Crystal Structure of $AlPO_4$-21, a Framework Aluminophosphate Containing Tetrahedral Phosphorus and both Tetrahedral and Trigonal-Bipyramidal Aluminum in 3-, 4-, 5-, and 8-Rings *Inorg. Chem.*, **1985**, *24*, 188–193.
45. Liu, Z.; Xu, W.; Yang, G.; Xu, R. New Insights into the Crystallization Mechanism of Microporous $AlPO_4$-21 *Micropor. Mesopor. Mater.*, **1998**, *22*, 33–41.
46. Tuel, A.; Jorda, J.-L.; Gramlich, V.; Baerlocher, C. Synthesis and Characterization of Two Aluminophosphates Templated by N-methyl-1,3-diaminopropane. *J. Solid State Chem.*, **2005**, *178*, 782–791.
47. He, H.; Klinowski, J. Solid-State NMR Studies of the Aluminophosphate Molecular Sieve $AlPO_4$-18. *J. Phys. Chem.*, **1993**, *97*, 10385–10388.
48. Jelinek, R.; Chmelka, B. F.; Wu, Y.; Grandinetti, P. J.; Pines, A.; Barrie, P. J.; Klinowski, J. Study of the Aluminophosphates $AlPO_4$-21 and $AlPO_4$-25 by ^{27}Al Double-Rotation NMR *J. Am. Chem. Soc.*, **1991**, *113*, 4097–4101.
49. Taulelle, F.; Loiseau, T.; Maquet, J.; Livage, C.; Férey, G. Oxyfluorinated Microporous Compounds. II. Solid State NMR of $(NH_4)_{0.88}(H_3O)_{0.12}AlPO_4(OH)_{0.33}F_{0.67}$ *J. Solid State Chem.*, **1993**, *105*, 191–196.
50. Taulelle, F.; Pruski, M.; Amoureux, J.-P.; Lang, D.; Bailly, A.; Huguenard, C.; Haouas, M.; Gérardin, Corine.; Loiseau, T.; Férey, G. Isomerization of the Prenucleation Building Unit During Crystallization of $AlPO_4$-CJ2: an MQMAS, CP-MQMAS, and HETCOR NMR Study. *J. Am. Chem. Soc.*, **1999**, *121*, 12148–12153.
51. Martineau, C.; Engelke, F.; Taulelle, F. Multiple Resonance Heteronuclear Decoupling under MAS: Dramatic Increase of Spectral Resolution at Moderate Magnetic Field and MAS Frequencies. *J. Magn. Reson.*, **2011**, *212*, 311–319.
52. MacKenzie, K. J. D.; Smith, M. E. *Multinuclear Solid-State Nuclear Magnetic Resonance of Inorganic Materials*, **2002**, Elsevier Science Ltd, Oxford, UK.
53. Pluth, J. J.; Smith, J. V.; Bennet, J. M. Microporous Aluminophosphate Number 17 with Encapsulated Piperidine, Topological Similarity to Erionite. *Acta Cryst.*, **1986**, *C42*, 283–286.
54. Tuel, A.; Lorentz, C.; Gramlich, V.; Baerlocher, C. AlPO-ERI, an Aluminophosphate with the ERI Framework Topology: Characterization and Structure of the As-Made and Calcined Rehydrated Forms *C. R. Chimie*, **2005**, *8*, 531–540.
55. Castro, M.; Seymour, V. R.; Carnevale, D.; Griffin, J. M.; Ashbrook, S. E.; Wright, P. A.; Apperley, D. C.; Parker, J. E.; Thompson, S. P.; Fecant, A.; Bats, N. Molecular Modeling, Multinuclear NMR, and Diffraction Studies in the Templated Synthesis and Characterization of the Aluminophosphate Molecular Sieve STA-2. *J. Phys. Chem. C*, **2010**, *114*, 12698–12710.
56. Tuel, A.; Caldarelli, S.; Meden, A.; McCusker, L. B.; Baerlocher, C.; Ristic, A.; Rajic, N.; Mali, G.; Kaucic, V. NMR Characterization and Rietveld Refinement of the Structure of Rehydrated $AlPO_4$-34. *J. Phys. Chem. B*, **2000**, *104*, 5697–5705.
57. Poulet, G.; Sautet, P.; Tuel, A. Structure of Hydrated Microporous Aluminophosphates: Static and Molecular Dynamics Approaches of $AlPO_4$-34 from First Principles Calculations. *J. Phys. Chem. B*, **2002**, *106*, 8599–8608
58. Antonijevic, S.; Ashbrook, S. E.; Biedasek, S.; Walton, R. I.; Wimperis, S. Yang, H. Dynamics on the Microsecond Timescale in Microporous Aluminophosphate AlPO-14 as Evidenced by ^{27}Al MQMAS and STMAS NMR Spectroscopy. *J. Am. Chem. Soc.*, **2006**, *128*, 8054–8062.
59. Cuny, J.; Xie, Y.; Pickard, C. J.; Hassanali, A. A. Ab Initio Quality NMR Parameters in Solid-State Materials Using a High-Dimensional Neural Network Representation. *J. Chem. Theor. Comput.* **2016**, *12*, 765–773.
60. Dawson, D. M.; Walton, R. I.; Wimperis, S.; Ashbrook, S. E. The Ambient Hydration of the Aluminophosphate JDF-2 to AlPO-53(A): Insights from NMR Crystallography. *Acta Cryst.* **2017**, *C73*, 191–201.

TOC Graphic